Icarus **139**, 189–201 (1999)
Article ID icar.1999.6095, available online at http://www.idealibrary.com on IDEAL®

Titan: High-Resolution Speckle Images from the Keck Telescope

S. G. Gibbard, B. Macintosh, D. Gavel, and C. E. Max

Institute of Geophysics and Planetary Physics, Lawrence Livermore National Laboratory, Livermore, California 94550
E-mail: sgibbard@beowulf.llnl.gov

I. de Pater

Department of Astronomy, University of California at Berkeley, California 94720

A. M. Ghez

Department of Physics, University of California at Los Angeles, California 90095

E. F. Young

Southwest Research Institute, Boulder, Colorado

and

C. P. McKay

NASA Ames Research Center, Moffett Field, California 94035

Received February 25, 1998; revised December 21, 1998

Saturn's large moon Titan is unique among planetary satellites in that it possesses a thick atmosphere and a haze layer that is opaque to visible light. This haze is believed to be composed of organic compounds produced by the photolysis of methane. It has been suggested that the photochemical products of methane photolysis, primarily ethane, would "rain out" over time and may produce reservoirs of liquid hydrocarbons on Titan's surface. Such material would appear very dark, with an albedo $\leq$0.02 (Khare *et al.* 1990, *Bull. Am. Astron. Soc.* 22, 1033). Such low-albedo regions have not been previously detected on Titan's surface. Here we report observations of Titan at a resolution of 0.04 arcsec (0.02 arcsec/pixel) using the technique of speckle imaging from the 10-m Keck I Telescope. By observing Titan at specific infrared wavelengths which are windows through its atmosphere, we have made both an albedo map of Titan's surface at 1.6 and 2.1 μm and an estimate of Titan's haze optical depth at these wavelengths. We clearly distinguish low-albedo features (reflectance $<$0.05) on Titan's surface.

Key Words: **Titan; infrared observations; surfaces, satellite.**

1. INTRODUCTION

Despite decades of observation, Saturn's largest moon Titan remains one of the most mysterious objects in the Solar System. Unlike other known planetary satellites, Titan possesses a thick (1.5 bars) atmosphere that like the Earth's, is composed mainly of nitrogen. It also contains small percentages of methane, hydrogen, and possibly argon. When observed by Voyager I in 1980 at visible wavelengths, only a featureless orange haze could be seen, with no hint of the surface underneath.

Titan's haze layer is produced by photolysis of methane in the upper atmosphere. The photolysis products combine into a complex series of organic molecules and polymers (Yung *et al.* 1984). These organics form a layer that is opaque at visible wavelengths and is partially transparent in the infrared. Calculations indicate that the methane in Titan's atmosphere would be depleted by photolysis on a time scale of 10^7 years (Yung *et al.* 1984), which indicates either that Titan's atmosphere is not in long-term steady-state (Lorenz *et al.* 1997), or that surface–atmosphere interactions replenish the atmospheric methane. It has been suggested that Titan may possess surface or subsurface reservoirs of liquid hydrocarbons produced by the raining out of methane photolysis products (Lunine *et al.* 1983).

Disk-integrated observations of Titan in the near-infrared (Griffith *et al.* 1991) indicate an atmosphere dominated by methane absorption features. Titan's surface can be observed through narrow windows of the methane spectrum in which light from the surface is not absorbed by the atmosphere. Because haze optical depth is less at infrared wavelengths than in the visible (Rages *et al.* 1983), it is easier to observe photons reflecting from the surface at 1.5–2.5 μm, where haze optical depths are generally less than 0.5, rather than at shorter wavelengths. The

0019-1035/99 $30.00

maximum contrast in surface features is greatly increased (to $\simeq$30%) at near-infrared wavelengths, compared to $\simeq$10% quoted by Smith *et al.* (1996) at the shorter wavelengths observed by the Hubble Space Telescope (HST). The values of contrast that can be obtained depend on both spatial and spectral resolution.

Unresolved, disk-averaged observations of Titan show variations in geometric albedo with time, as well as a north/south brightness asymmetry that is believed to be due to seasonal transport of Titan's haze particles (Hutzell *et al.* 1993, 1996). Daily variations are due to a brightness difference between Titan's leading and trailing hemisphere (the leading hemisphere being brighter) as Titan revolves around Saturn with a period of 15.95 days (Lemmon *et al.* 1995). Longer time variations involve a north/south brightness asymmetry and occur with a period of $\simeq$30 years, consistent with the orbital period of Titan around the Sun (Lockwood *et al.* 1986). This asymmetry currently has the opposite sign from that observed 18 years ago by Voyager 1.

Titan has been observed in visible and near-infrared windows by the HST (Smith *et al.* 1996) and in the infrared using adaptive optics technology (Combes *et al.* 1997). These observations have confirmed the brightness asymmetry between Titan's leading and trailing hemispheres, as well as the north/south brightness asymmetry. The diffraction-limited resolution achieved by the HST at 0.9 μm was 0.09″ (0.045″ per pixel) and by adaptive optics 0.14″. The deduced surface characteristics indicate a heterogenous surface rather than the global hydrocarbon ocean suggested by loss of methane to the surface at the current rate over the age of the Solar System (Yung *et al.* 1984, Lara *et al.* 1994).

Early radar measurements of Titan's albedo (Muhleman *et al.* 1991) suggested a radar reflectivity much too high for liquid hydrocarbons and more consistent with an icy surface. The early values reported by Muhleman *et al.* (1991) were later revised down by a factor of $\sim$2 (Muhleman *et al.* 1995), due to an error in the calibration procedure (for details see de Pater *et al.* 1994). In contrast to the early reports, the radar reflectivities are therefore not inconsistent with a surface that is covered to some extent by solid or liquid hydrocarbons (Lorenz and Lunine 1997).

It now seems clear, from both observations and theory, that Titan does not possess a *global* hydrocarbon ocean (Sears 1995, Sagan and Dermott 1982, as well as the infrared and HST data mentioned above). However, it is quite possible that smaller reservoirs of liquid ("seas") exist on Titan but have not been detected by previous observers. Unambiguous detection would require very high-resolution measurements to separate the heterogenous areas of the surface as well as high-spectral resolution to positively identify the surface components.

In order to help answer such questions, we have used the technique of speckle imaging on the world's largest optical telescope, the W. M. Keck 10-m Telescope, to produce infrared images of Titan at a higher spatial resolution than previous images taken at any wavelength. In addition to producing images of the surface, we have used the data to constrain models of Titan's atmospheric haze layer.

2. OBSERVATIONS AND DATA REDUCTION

Observations were taken on June 27 and September 6, 1996 (UT) using the 10-m W. M. Keck Telescope and the 256 $\times$ 256 pixel NIRC camera (Matthews and Soifer 1994) in speckle imaging mode (Matthews *et al.* 1996). In this mode, a warm image converter provides NIRC with a plate scale of 0.02 arcsec per pixel. This plate scale gives approximately 40 pixels (20 resolution elements) across the disk of Titan. The K′ observations have a spatial resolution of 0.04 arcsec, which is $\simeq$260 km on Titan's surface, a higher spatial resolution than any previous observations.

Our observations in June were primarily of Titan's trailing hemisphere (Titan orbits synchronously around Saturn, so that its leading and trailing sides are always imaged at greatest eastern and western elongation). The central meridian longitudes at the time of observation were 125° for the leading hemisphere and 320° for the trailing hemisphere. The data from September show the leading, brighter hemisphere. Data from June were obtained in the K′ band (1.95–2.29 μm), and data from September at both K′ and H (1.49–1.82 μm). These wavelength ranges include both strong methane absorption bands and windows where methane absorption is nearly zero, so that light can penetrate to the surface.

The observations taken are summarized in Table I. Each data set consists of 100 images, with a 0.200-s exposure time per image. Each such stack typically takes 90 s to complete. Each frame also has 8 (June) or 200 (September) dark/bias exposures associated with it, which are used to calibrate drifts in the DC bias level of NIRC's electronics. The number of dark/bias exposures was increased in September because the time-varying bias and read noise in the dark frames were dominant noise sources in the June data.

Before the speckle analysis procedure began, the data were preprocessed as conventional infrared images. The instrument dark current and (time-varying) bias were removed using bias frame stacks associated with each data set. Data were sky-subtracted using 300-frame blank-sky observations taken shortly before or after the Titan and reference images. A median filtering technique was then applied to each image to remove residual columnar patterns caused by drifts in the instrument electronics. The resulting images were flat-fielded using flats constructed from twilight sky images.

Figure 1 shows the images obtained from speckle reconstruction of the data. Figure 1a is the leading hemisphere at K′, reconstructed from 5 sets of 100 speckle frames that were shifted to a common center and averaged to produce the image. Figure 1b shows the leading hemisphere at H band, reconstructed from an average of 4 sets of 100 speckle frames, and Fig. 1c shows the trailing hemisphere at K′, reconstructed from 2 sets of 400 speckle frames. Near the center of the satellite, infrared photons pass through only a thin layer of reflective haze and either are absorbed by the methane below the haze or reach the surface. On the other hand, near the limb the pathlength through the

TABLE I

Data Set	Object	Filter	Time(UTC)	Parallactic Angle	Reference Star Set(s) [2]
June 27, 1996					
709	Titan	K'	14:25:12	55.37	749,758,767
718	Titan	K'	14:27:46	54.85	749,758,767
727	Titan	K'	14:30:03	54.38	749,758,767
736	Titan	K'	14:32:32	53.85	749,758,767
749	SAO 109256	K'	14:37:26	54.33	n/a
758	SAO 109256	K'	14:39:59	53.76	n/a
767	SAO 109256	K'	14:42:23	53.21	n/a
825	Titan	K'	15:04:59	45.08	749,758,767
834	Titan	K'	15:07:31	44.23	749,758,767
843	Titan	K'	15:10:05	43.33	749,758,767
852	Titan	K'	15:12:47	42.35	749,758,767
September 6, 1996					
342	SAO 188588	H	08:46:22	-32.53	362
362	SAO 188549	H	09:27:47	-43.30	n/a
458	Titan	K'	11:31:19	7.92	490
473	Titan	K'	11:46:38	-2.57	490
476	Titan	K'	11:51:55	-6.18	490
483	Titan	K'	11:58:00	-10.29	490
490	SAO 128780	K'	12:05:10	-11.73	n/a
517	SAO 128735	K'	12:44:05	-35.97	490
524	Titan	K'	12:50:45	-38.81	517
604	SAO 128762	H	14:44:05	-62.18	n/a
614	Titan	H	14:56:42	-64.19	604
617	Titan	H	15:01:48	-64.62	604
620	Titan	H	15:06:40	-65.01	604
623	Titan	H	15:11:33	-65.38	604

[1] UTC time from instrument control computer, which contains an unknown offset of several seconds relative to true UTC.
[2] Data set used for speckle calibration (see Section 3).

high-altitude haze is longer and photons have a greater chance of being scattered or reflected before they reach the absorbing methane layer. This, combined with a greater amount of haze in the southern hemisphere, leads to a strong southern limb brightening. The observed limb brightening is used to constrain models of the atmosphere.

3. SPECKLE IMAGE RECONSTRUCTION

Titan is difficult to analyze from the ground because of its small angular size, about 0.8 arcsec in diameter. This is roughly the size of the point spread blurring caused by turbulence in the Earth's atmosphere. Consequently, most ground-based observations prior to 1996 measured only properties of the integrated disk.

Since then, high-resolution techniques have been developed that can to a certain degree overcome the atmosphere and reach a resolution limit set by the diffractive properties of the telescope optics. The diffraction limited resolution varies directly with telescope diameter, so the larger (e.g., Keck 10-m) telescopes on the ground can in theory obtain higher resolution than HST, with its 2.4-m aperture in space. Adaptive optics results at ESO (Combes *et al.* 1996) with a 3.6-m telescope have yielded disk-resolved images in the infrared windows and confirmed that Titan rotates synchronously around Saturn.

Speckle imaging is a high-resolution technique that works well on bright objects such as Titan. The idea is to take very short exposures ($\simeq$100 ms) to "freeze" the atmospheric turbulence and capture the light while it is still forming coherent interference patterns at the detector. The coherence patterns

contain diffraction-limited information that can subsequently be used to determine the object's Fourier amplitudes and phases, which are combined with an inverse Fourier transform to produce a diffraction-limited image. Algorithms for the recovery of diffraction-limited information were first introduced by Labeyrie (1970) for computing the Fourier amplitudes, or equivalently the autocorrelation of the image, and extended to full image recovery by Knox and Thompson (1974), Weigelt (1977), Lohmann *et al.* (1983), and Roddier (1986), who recognized the similarity of the bispectrum imaging method to phase closure techniques in radio interferometry. Speckle imaging has been widely used to make measurements of binary stars (e.g., McAlister *et al.* 1984, Henry and McCarthy 1993), study T-Tauri stars (e.g., Ghez *et al.* 1995, Leinert *et al.* 1993, Koresko *et al.* 1991), image solar features (e.g., Von der Luehe 1994), image galactic nuclei (e.g., Olivares 1994, Thatte *et al.* 1997), and image planetary objects (e.g., Beletic 1992, McCarthy *et al.* 1994, Max *et al.* 1996).

Data are postprocessed using the power spectrum and bispectrum speckle image reconstruction algorithms, which consist of Fourier transforming each frame and averaging the squared magnitude of the transforms to obtain the image power spectrum in the spatial frequency domain and applying the triple-correlation algorithm (Lohmann *et al.* 1983), with modifications by Lawrence *et al.* (1992) to obtain the object phase in the spatial frequency domain. Titan's spatial frequency power spectrum is recovered from the image power spectrum through division by the average power spectrum of the reference stars, with corrections for noise biasing (Lawrence *et al.* 1992).

In order to avoid calibration problems related to the rotation of the telescope pupil, the speckle frames were obtained with the telescope's image rotator in the stationary mode, so that the telescope pupil remained fixed. This caused the image to rotate as the telescope tracked the object. We therefore derotated the images reconstructed from individual sets of 100 frames, placing Titan's north pole along the $+y$ direction. The blurring caused by the image rotation during the individual frame sets was never greater than 0.25 pixels anywhere on Titan's disk.

The reconstructed images clearly show a diffraction-limited spatial resolution of 0.04 arcsec (because of the pixel size of 0.02 arcsec, the resolution at H band is limited by Nyquist sampling to 0.04 arcsec rather than the theoretical limit of 0.03 arcsec). Further cross-checking of the reconstruction, along with an indication of the level of image artifacts, is accomplished by applying the algorithm to test stars not used in the deconvolution step. We found that the technique left residual artifacts at about the 5% level of contrast. The implication is that measurements of brightness, and indirectly, surface reflectance, in dark regions are trustworthy to an upper bound of 5% of the brightness of the bright regions.

We measured an apparent magnitude for Titan of 8.18 ± 0.1 at 2.1 μm and 8.04 ± 0.1 at 1.6 μm. This gives a geometric albedo of 0.057 at 2.1 μm and 0.07 at 1.6 μm. This is consistent with measurements made by previous observers (Griffith *et al.* 1991).

4. ATMOSPHERE MODEL

In order to separate the contributions of light due to atmospheric scattering and light reflected from the surface, we used a radiative transfer model that simulates the absorption, reflection, and scattering of photons from Titan's atmosphere and a constant-albedo surface (Toon *et al.* 1989). This model has previously been applied to Titan by Toon *et al.* (1992) and Hutzell *et al.* (1993, 1996). The model uses a computationally efficient algorithm to solve the two-stream approximation in an inhomogeneous multiple-scattering atmosphere. The Eddington method is used to determine the two-stream coefficients. The accuracy of this method is usually better than 10% for the calculation of radiative streams, except for large solar zenith angles where the error may reach 10–20%. Since other sources of error (e.g., the values of the scattering coefficients determined from fractal particle models) are not known to better than 10–20%, this provides sufficient accuracy for our purposes.

We assume that the atmosphere does not vary in longitude and varies smoothly with latitude as described below. We fit the data as well as possible to such an atmosphere, in particular near the limb of Titan, where the intensity is dominated by atmospheric scattering and is essentially independent of the surface albedo. Any residual that remains when we remove this atmosphere from the data is assumed to be due to surface features. The atmosphere is divided into three vertical layers, each of which has a value for the haze and gas optical depths. The haze is confined to the top two layers, with methane underneath. Models with more layers (up to 10) were also tried, with results similar to the three-layer model. The methane is assumed to be completely absorbing within the fraction of the filter that is in the methane band (this fraction is 61% for K′ and 69% for H), and to be transparent outside of the methane absorption band. Haze single scattering albedos and forward/backward scatter asymmetry factors at H and K′ band (given in Table II) are derived from a fractal model of Titan's haze particles (Rannou *et al.* 1995). In order to account for the observed north/south haze asymmetry, the haze optical depth was assumed to decrease linearly from the southern limb to the equator, and from the equator to the northern limb using independent slopes for each hemisphere.

Our standard model assumes that the surface of Titan reflects as a Lambert disk; this is a surface for which the reflected intensity varies as the cosine of the angle from the disk center. This is only one extreme in the possible continuum of reflectance models. The opposite extreme is a more lunar-like pattern in which the reflectance does not vary across the disk. We have also constructed models with a constant reflectance (which will be referred to as "lunar-like") to test the sensitivity of the models to this unknown parameter. As might be expected, since the lunar-like surface reflects more efficiently at high zenith angles, the effect of using a lunar-like model is to produce a somewhat lower surface reflectance at the edges of the disk; the central values are essentially unchanged. The best-fit values of the haze optical

depth for the lunar-like models are slightly less at the north and south poles (e.g., 0.26 vs 0.3 at the south pole and 0.06 vs 0.1 at the north pole for the K′ band). In theory it would be possible to use these models to determine whether Titan's surface is indeed more "Lambert-like" or "lunar-like"; however, we do not find enough difference between the results of the two models to make this distinction.

The modeling process produces a theoretical image of Titan's atmosphere with effectively infinite spatial resolution. To compare this to our observations, the model must be degraded to the true resolution of our images, by convolving it with the point spread function (PSF) of our data. In the case of perfect speckle data, with infinite signal-to-noise and no systematic calibration errors, the point spread function would simply be the inverse of the modulation transfer function (MTF) of the telescope—an Airy disk for a round telescope, a somewhat more complex shape for the hexagonal Keck primary mirror. In practice, noise in the data (which becomes significant at high spatial frequencies in the power spectrum) and calibration errors (due to changes in the atmospheric turbulence properties between the images of Titan and the images of the PSF reference star) will degrade the resolution of the images.

We estimated this degradation at K′ band by speckle-processing images of one star—SAO 128735—in the same fashion as our Titan data, using a different star as a reference (See Table I). (A similar PSF, constructed from observations of 188588, was used for the H-band data.) The resulting PSF was then used to convolve our models. Inspection of the resulting image, particularly the brightness profile of the image in the area beyond Titan's limb (which will depend primarily on the PSF, not the model), indicated that the actual Titan data were sharper than the SAO 128735 data. This is most likely due to fluctuations in the atmospheric properties ("seeing") over the course of the observations; if the SAO 128735 observations were taken in a time of slightly worse seeing than the SAO 128780 observations used for the speckle processing, the resulting image would be slightly blurred. Conversly, convolving the model with the theoretical "perfect" PSF produced an image that was clearly sharper than our actual observations. We therefore developed a mixed PSF produced by a weighted average of the star/star PSF and the theoretical PSF. We evaluated the goodness-of-fit by comparing the brightness profile beyond the limb of the convolved model with our observations; since the model naturally has no flux beyond its limb, the shape of the convolved image in this region is dependent only on the PSF used. All these deviations from the theoretical PSF are relatively small—the images all achieve the 0.04" diffraction limit, with the variations being in the amount of light present in a low-level halo surrounding the central core. A 50% theoretical/50% observed PSF weighting was found to produce results that most closely correspond to our observed data. The effect of varying the PSF on the total haze opacity is relatively small; the best-fit model with the theoretical PSF has a total haze opacity in the southern hemisphere of 0.26, compared with 0.3 using the composite PSF. The effect on the surface reflectance was small—an increase in reflectance of 0–0.02 across the disk, with the largest effect near the limb. The reflectance of the dark regions remained below 0.05.

Once the model was corrected for the point spread function of the data, there were two main steps to the fitting process. First, the atmospheric parameters—particularly the optical depth in the scattering haze—were determined by fitting a model with uniform surface albedo to the limb of our observations. Second, those haze parameters were used to recover a surface reflectance map by removing the contribution to the light due to the atmosphere and by correcting for absorption and scattering of surface light.

In the first step, a series of models with varying haze optical depths and surface albedos was generated. The albedo was assumed to be uniform across Titan's surface. This is clearly not the case. However, since the "goodness-of-fit" of each model was evaluated primarily in the limb regions, this means we are merely assuming that the albedo in the southern and northern polar regions is relatively uniform. In both our observations and other groups' studies of Titan (Smith *et al.* 1996, Combes *et al.* 1997) the southern and northern polar regions appear devoid of bright features. In addition, the assumed albedo couples only weakly into our atmospheric model for two reasons. First, the limb emission is clearly dominated by scattered light from haze, particularly in the south, as can be seen from the sharp limb brightening; the relative contribution due to haze is further magnified since our observations span a wavelength range that only partially probes the surface. Second, due to the absorption and scattering of light reflected from the surface on the way up, the overall brightness at the limb is only a weak function of the assumed surface albedo.

The model parameters—haze optical depth as a function of latitude and (uniform) surface albedo—were adjusted to produce the model that best fit our observations for several longitudinal slices 5 pixels wide near the northern and southern limbs (Figs. 2a–2c). We consider our recovered optical depths to be good to ±20%; a model with 20% less haze clearly undersubtracts the limb brightening while a model with 20% more haze clearly oversubtracts (Figs. 2d and 7).

Figure 2 shows plots of brightness as a function of image row for three vertical (N/S) slices through our image. It can be seen that the model reasonably fits the data near the limbs. Away from the limbs, deviations from the model are presumably due to nonuniform surface albedo; in particular, the region where the data are well below the model in Fig. 2c indicates a surface reflectance that is well below the uniform 0.05 reflectance used in this model.

Once the best-fit haze parameters were determined, the model was used to generate an "atmosphere-only" map with an assumed surface albedo of zero (Fig. 3). This atmosphere-only map was then separated from our data to produce an image of the residual emission, due to the (nonuniform, nonzero) surface. The map was then corrected for atmospheric absorption and

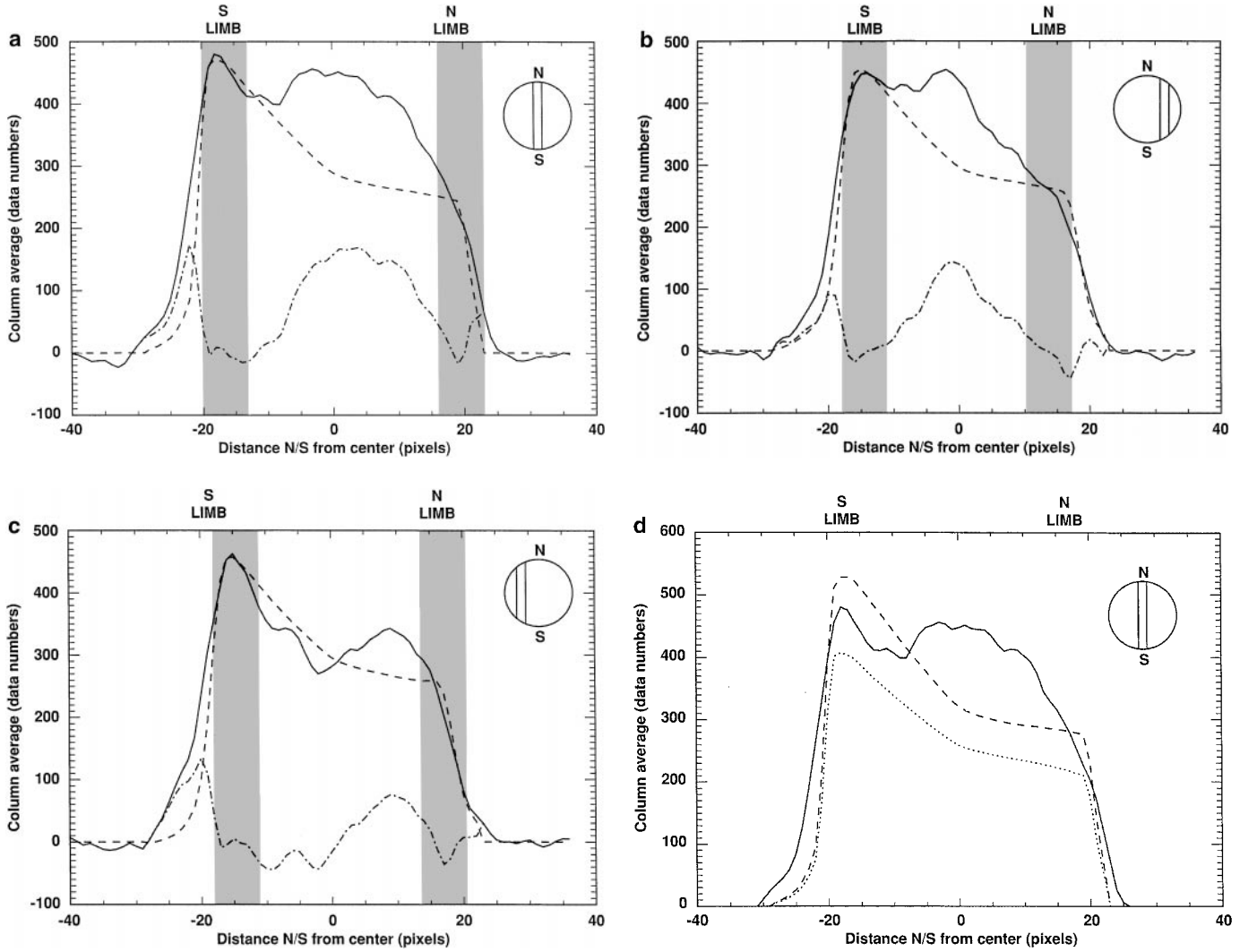

FIG. 2. Fitting the model to the data. (a–c) show N/S slices (average of 5 pixels) through the satellite at three different longitudes compared to the average of 5 pixels of the model atmosphere plus a surface with a constant albedo of 0.05. The solid line is data, the dotted line is the model, and the dot–dash line is the residual (difference between data and model). Data are fit to the northern and southern limbs (hatched areas). The positive residual near the center of the image is due to a bright surface feature, the negative residual in (c) (just north of the southern limb) is one of the dark regions. (d) shows a center N/S slice of the data (solid line), an atmosphere model with 20% less haze than the nominal value (dotted line), and 20% greater haze (dashed line). These models are clearly less adequate fits to the northern and southern limbs than the nominal model shown in (a–c). The surface reflectance produced by the 20% greater and 20% less haze models is shown in Fig. 7.

scattering and angle-of-incidence effects (assumed to be Lambertian) by comparing it to a model with a constant surface albedo. In modeling our data for the trailing hemisphere at K′ band, which has lower signal-to-noise than the leading hemisphere data, we have used the atmosphere parameters which best fit the leading hemisphere. Along with the leading hemisphere models at H and K′ bands, this gives the surface reflectance maps shown in Fig. 6. We note that, according to our model, 28% of the light from the planet comes from the surface (on a disk-averaged basis) at H band, and 30% at K′. The remainder of the light is reflected from the haze.

5a. RESULTS: ATMOSPHERE

Table II shows the deduced haze optical depths in the K′ and H bands. These results are not in complete agreement with either of two previous globally averaged models (Fig. 4). The fractal haze particle model of Rannou *et al.* (1995) has about twice the global average optical depth obtained from our analysis while the earlier spherical particle model (McKay *et al.* 1989) gives a value about four times greater. Our results also indicate that Titan's haze optical depth currently (as of 1996) varies by a factor of $\simeq$3 from south to north.

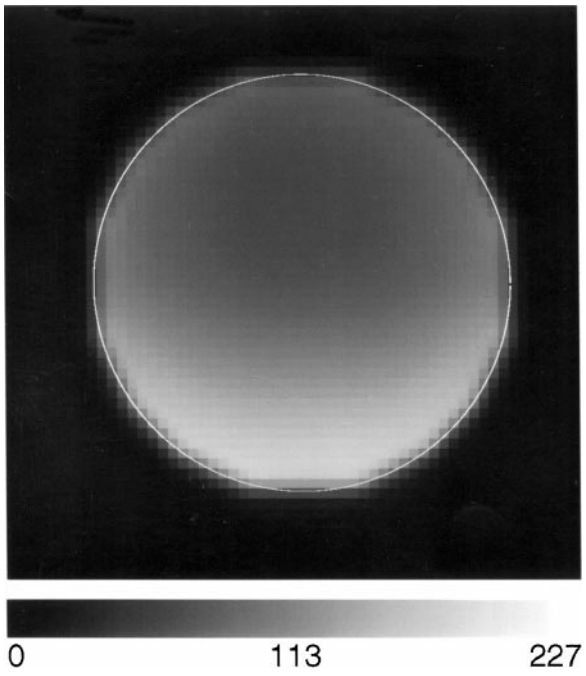

FIG. 3. Brightness of a Titan model atmosphere at K′ band shown in grayscale map. Units of scale are flux in 10^{-18} Watts/m^2/μ/pixel (same units as Fig. 1). This image is for a surface albedo of zero, so that all light comes from the atmosphere. The model for H band is very similar. Strong southern limb brightening is due to higher haze abundance in the southern hemisphere.

TABLE II
Values for Scattering Parameters and Best-Fit Haze Optical Depths at 1.6 and 2.1 μm

Wavelength	g	ω	τ_S	τ_E	τ_N
1.6 μm	0.40	0.97	0.45	0.23	0.14
2.1 μm	0.20	0.85	0.30	0.15	0.10

Note. g = scattering asymmetry factor, ω = single-scattering albedo, τ_S = haze optical depth at southern limb, τ_E = haze optical depth at equator, and τ_N = haze optical depth at northern limb. Values for g and ω were taken from the fractal haze particle model of Rannov *et al.* (1995). Haze optical depth is assumed to decrease linearly from the southern limb to the equator and from the equator to the northern limb).

Both the spherical and the fractal haze models shown in Fig. 4 are adjusted to fit the geometric albedo of Titan in spectral range from 0.3 to 0.9 μm. The opacity of the atmosphere at longer wavelengths is an extrapolation from this fit. For spherical particles more mass of haze is needed to fit the visible than for the fractal model because the optical cross section of the fractal particles is larger per unit haze mass than for spherical particles. However, at longer wavelengths, where the absorption and scattering are in the Rayleigh regime, the optical cross section is more nearly proportional to the total haze mass and is not sensitive to the particle shape. Thus, the fractal optical depth falls below the spherical optical depth in the infrared.

Our data indicate that the optical depths in the infrared are somewhat lower than predicted by the fractal model. This could

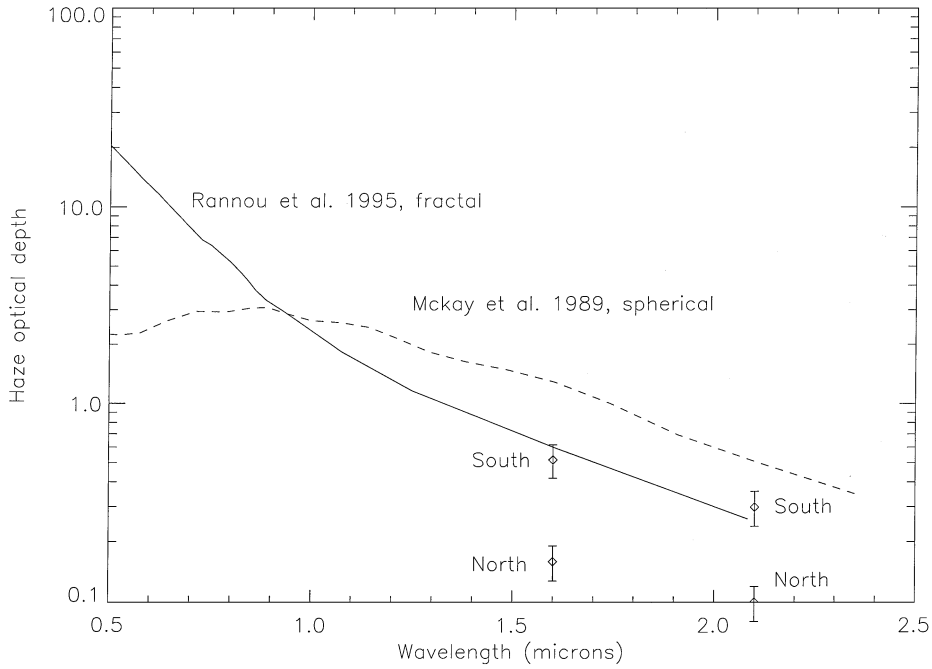

FIG. 4. The optical depth of Titan's haze layer at various wavelengths. Two models are shown: the Mckay *et al.* (1989) spherical particle model and the Rannou *et al.* (1995) fractal particle model. Data are shown for H and K′ band; numbers are given for the value found at the northern and southern limbs along with 20% error bars.

indicate that the fractal model is still not an adequate representation of Titan's haze either because the fractal dimension used ($D = 2$) is incorrect or the basic assumption of radial symmetry of the fractal particles is not valid. Many condensates do form string-like aggregates that could have significantly different optical properties than the fractal models of Rannou *et al.* (1995). Also, a portion of the difference may be due to seasonal variations between our observations and the Rannou *et al.* data. We note that our haze optical depth values at 2 μm (particularly in the northern hemisphere of Titan) are in good agreement with the results of Griffith *et al.* (1991), who found a disk-integrated haze Mie scattering optical depth at 2 μm of 0.1–0.13.

Knowledge of Titan's haze optical depth at infrared wavelengths is useful for comparing and refining models of the structure of Titan haze particles (Rannou *et al.* 1995, McKay *et al.* 1989), which can then be used to extrapolate haze optical depths to other wavelengths (see Fig. 4). The Cassini mission to Saturn, launched in October 1997 and scheduled for arrival in 2004, carries the Imaging Science Subsystem (ISS), a CCD imaging system with the potential of acquiring images of Titan's surface with spatial resolutions of tens of meters. The ISS carries a 0.94-μm filter tuned to the methane window expressly for imaging the surface and a polarizer to help block singly scattered photons, but the proportion of nonscattered photons reflected from the surface is a steep function of the haze optical depth. Multiply scattered photons have the potential to severely degrade the spatial resolution of the ISS, possibly blurring features to as much as several kilometers. The H and K′ haze optical depths determined from our Keck speckle observations, combined with future shorter wavelength optical depth measurements, can be used to refine performance constraints for the Cassini ISS.

Our results indicate optical depths lower than predicted by either the fractal or spherical particle models, which is good news for the Cassini mission. These lower optical depths imply that the surface can be easily imaged in the 1-μm methane window, albeit with the caveat that there could be low-level haze which is not included as a separate parameter in our model.

5b. RESULTS: SURFACE

Titan's surface albedo provides clues to its surface composition. Suggested surface compositions range from liquid hydrocarbon oceans (Lunine 1983) to solid rock or ice/hydrocarbon mixtures (Muhleman *et al.* 1991, Griffith *et al.* 1991). Figure 5 shows the surface reflectance of Titan's leading hemisphere at K′ band in a false-color map. Figure 6 shows surface reflectance for both leading and trailing hemispheres at K′ and for the leading hemisphere at H. Titan's surface is clearly heterogenous, with bright areas of reflectance >0.15 in the H band and very dark areas with reflectance <0.05 at both H and K′. The surface images have an average reflectance for the September image (45° away from the usual "bright side" reported in the literature) of 0.059 ± 0.027 at 2.0 μm with an equivalent geometric albedo of 0.046 ± 0.018. This is higher than $2/3$ of the average reflectance since the bright feature is relatively central. At 1.6 μm the average reflectance is 0.085 ± 0.04 and the equivalent geometric albedo 0.066 ± 0.027. In June—centered on the dark side of Titan—the average 2.0-μm reflectance is 0.027 ± 0.027 and the geometric albedo is 0.023 ± 0.018. If we neglect the outermost 5-pixel annulus of each map (which is most sensitive to errors in the atmosphere fitting, but also favors the brighter terrain) we get average reflectances of 0.079 ± 0.023, 0.111 ± 0.034, and 0.038 ± 0.023 for September 2.0 μm, September 1.6 μm, and June 2.0 μm, respectively.

These results can be compared to disk-integrated infrared albedos from previous observers, which are summarized in Lorenz and Lunine (1997). The previous data show a wide range of albedo values both for Titan's bright (leading) and dark (trailing) hemispheres. For example, values given for the geometric albedo of the bright hemisphere at 1.6 μm range from 0.07 (Griffith *et al.* 1991) to 0.4 (Lemmon *et al.* 1995). Past spectroscopic studies of Titan's surface have provided differing results primarily because of photometric errors associated with narrow slit spectroscopy. At this time it is difficult to say which values are most accurate, although our values appear to be in reasonable agreement with Griffith *et al.* (1991).

Previous observations have not detected the regions we find on the leading hemisphere with infrared reflectance <0.05, presumably because these regions have a modest spatial extent and have been blurred by scattered light from the brighter regions at lower spatial resolution. To test our conclusion that these regions are very dark, we have constructed atmospheric models with a 20% lower haze optical depth (Fig. 7a). These models, which have a clearly undersubtracted southern limb, still have a reflectance in the dark region of ≤ 0.05. Models with a 20% higher haze optical depth produce dark regions with reflectance <0 (Fig. 7c). We therefore are confident that these regions are very dark at both H and K′ bands. These regions could be larger than our map indicates, covering most of the area to the left of Fig. 5 (west in Titan coordinates) if we have either underestimated the haze optical depths in the north, or if the PSF scatters significant light from the bright feature.

6. DISCUSSION AND INTERPRETATION OF SURFACE FEATURES

The reflectances we have obtained here for Titan's surface may be compared to those of other Solar System bodies and laboratory materials in order to narrow the range of candidate materials. Table III lists the geometric albedos of some Solar System bodies and of other Titan surface candidate materials at 1.6 and 2.1 μm.

From a comparison of Figs. 6a and 6b it can be seen that the bright region on the leading hemisphere is somewhat brighter at H than at K′, which suggests that it may be composed of water-ice (which is dark at 2 μm and somewhat brighter at 1.6), or an ice–rock mixture. The bright feature has a similar spatial extent

TABLE III
Albedos of Candidate Materials

Object	*1.6μm albedo*	*2.1μm albedo*
Europa[a](ice)	0.25	0.11
Moon[b](rock)	0.3	0.3
Iapetus (dark regions)[c]	0.11	0.10
Phoebe[d]	0.06	0.05
C-type asteroids[e]	0.04-0.06	0.04-0.06
Titan tholin[f]	0.06-0.08*	0.06-0.08*
liquid hydrocarbons[g]	< 0.02*	< 0.02*
Titan dark areas (this work)	< 0.05*	< 0.05*
Titan bright areas (this work)	$0.12 - 0.18$*	$0.10 - 0.13$*

* These numbers are normal reflectance values; all others are geometric albedos.

[a] Clark and McCord (1980).
[b] Lorenz (1997).
[c] Lebofsky *et al.* (1982).
[d] Degewij *et al.* (1980), scaled to values from Tholen and Zellner (1983).
[e] Tholen and Barucci (1989).
[f] Khare *et al.* (1984).
[g] Khare *et al.* (1990).

to the bright region seen by other observers (Smith *et al.* 1996, Combes *et al.* 1997), and we find, in agreement with previous observations (Combes *et al.* 1997), that the bright region has "peaks" with reflectance 10–15% greater than the surrounding bright regions. The general shape of the bright region, including the westward extension near the north pole in Fig. 5, is quite similar to that seen by the HST at a wavelength of 0.94 μm (Smith *et al.* 1996).

The trailing hemisphere of Titan at the K′ band has an overall brightness less than the leading hemisphere, and we again find (Fig. 6c) that the albedo is not uniform. The trailing hemisphere shows features qualitatively similar to those observed by Combes *et al.* (1997), namely, that there is a somewhat brighter region in the northern hemisphere (reflectance $\simeq$0.07), and a less bright feature (reflectance $\simeq$0.05) in the southern hemisphere.

The reflectance of the very dark regions is too low for water-ice such as is seen, for example, on Jupiter's moon Europa, although very smooth ice, which would appear dark in the infrared, remains a possibility. Another possibility, that the dark material could consist of deposits similar to those found on the other saturnian satellites Iapetus and Hyperion, is unlikely since the Iapetus dark material is too bright in the infrared (Vilas *et al.* 1996).

Saturn's satellite Phoebe, on the other hand, is quite dark in the infrared. Phoebe is believed to be a captured asteroid because of its spectral similarity to C-type asteroids (their infrared albedo is similar; see Table III). However, even Phoebe-like material is not as dark as the darkest regions we observe on Titan's leading hemisphere. Another possibility is that the dark material is similar to laboratory-produced "tholins" (Khare *et al.* 1984), perhaps mixed with water-ice. However, the reflectance of "tholins" is in the range of 0.06–0.08, probably too high to explain the very low reflectance of the dark regions on the lower left quadrant of Fig. 5.

In theory, these patches of material could also have an extra-Titan source, such as asteroidal dust. However, because of Titan's thick atmosphere, any dust falling in from outside the atmosphere would be spread rather evenly over Titan's surface. We cannot envision a scenario where much material would naturally accumulate in restricted patches on the surface.

Finally, we note that the localized areas of dark material could be the elusive "lakes" or "seas" of liquid hydrocarbon that have long been predicted to exist on Titan's surface. We find that the reflectance of these regions is sufficiently low at 1.6 and 2.1 μm that the presence of liquid hydrocarbons cannot be ruled out. If photochemical models (Lara *et al.* 1994) are correct, the amount of liquid found in these regions is probably not enough to keep the atmosphere resupplied with methane.

In view of the many possibilities for Titan's surface composition, it is useful to discuss what the distribution of bright and dark regions evident at high resolution can tell us. The dark material on Titan's leading hemisphere appears to be restricted to confined areas. Compared to features on the Earth, the size of the dark area seen in the lower left of Fig. 5 is about as big as Hudson's Bay, and somewhat larger than the Black Sea. The dark areas may be large basins (impact or volcanic basins) that are covered by dark material which comes from the interior of the satellite or is brought in by a dark impactor (which would probably be vaporized in the process). Since Titan is a differentiated object, it is hard to see how material that appears to be most similar to primitive asteroids could be indigenously present on its surface, particularly only in restricted areas. If liquid hydrocabons exist on Titan's surface, the bright and dark patterns could be due to the redistribution of liquid to low-lying areas. Or the surface of Titan could be continually covered by dark material precipitating out from the atmosphere, which is washed from only the higher lying (bright) areas by methane rain, exposing bright ice underneath (Griffith *et al.* 1991).

FIG. 1. Speckle processed images of Titan. (a) shows the leading hemisphere at K′ (2.1 μm); (b) is the leading hemisphere at H (1.6 μm), and (c) is the trailing hemisphere at K′. The central longitude for the leading hemisphere is 125° and for the trailing hemisphere 320°. Titan north is up and west is to the left. The mapping of intensity to color is the same for (a) and (c); (b) has a different color mapping since Titan's integrated intensity is greater in the H band. Units of scale are flux in 10^{-18} Watts/m^2/μ/pixel.

FIG. 5. False-color map of Titan's surface reflectance in the K′ band, showing the leading hemisphere (central longitude 125°).

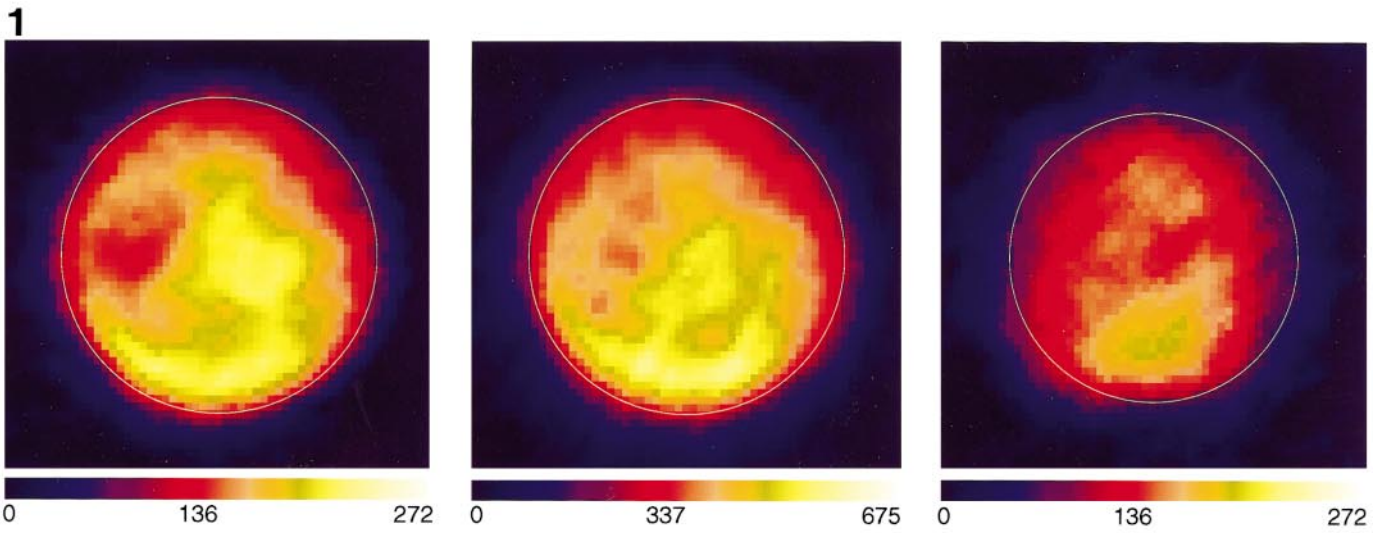
1
0
136
272
0
337
675
0
136
272

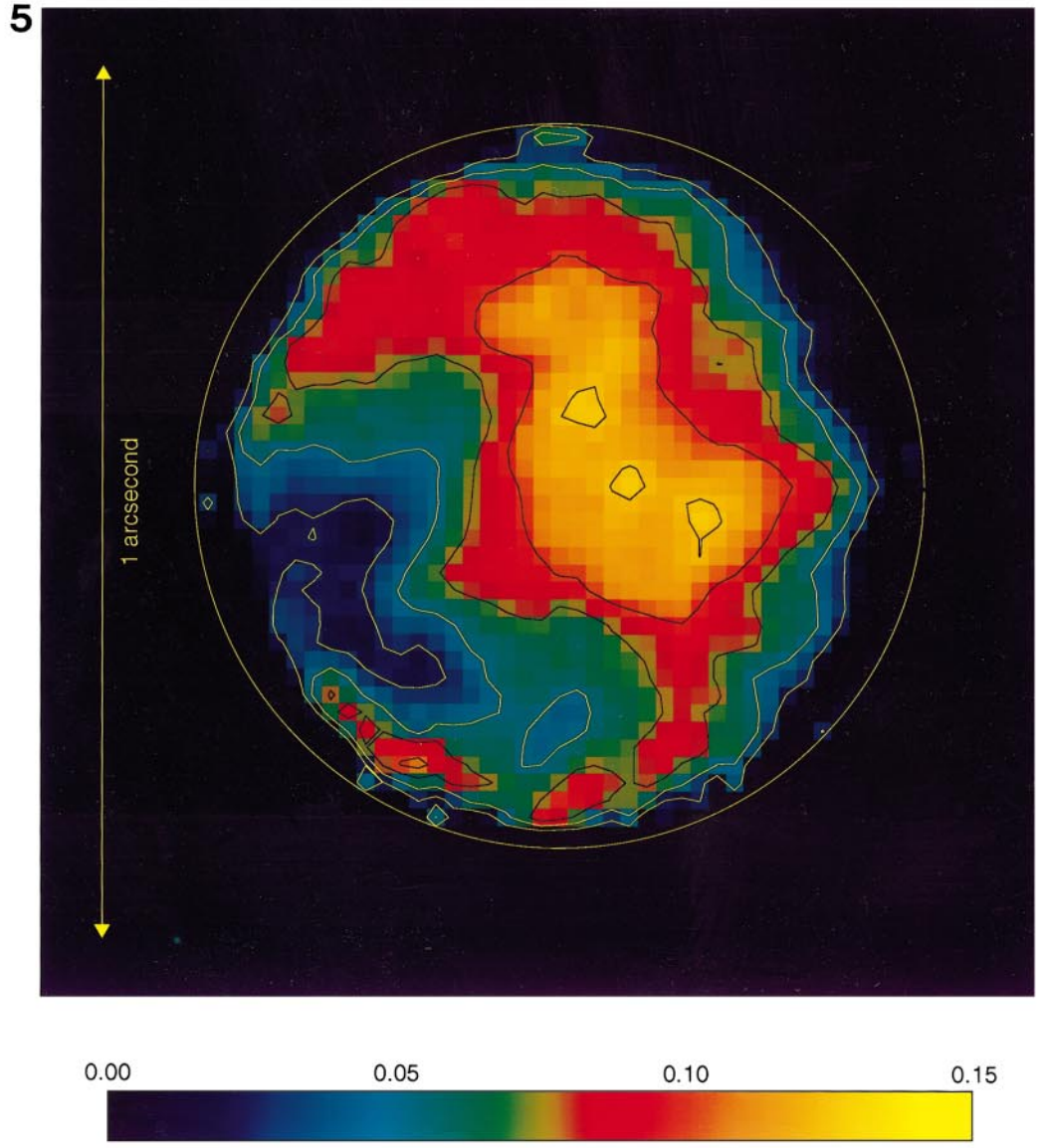
5
1 arcsecond
0.00
0.05
0.10
0.15

Recovered Titan Surface Albedos

6

6a. 2.1 μm reflectance (Leading) 6b. 1.6 μm reflectance (Leading) 6c. 2.1 μm reflectance (Trailing)

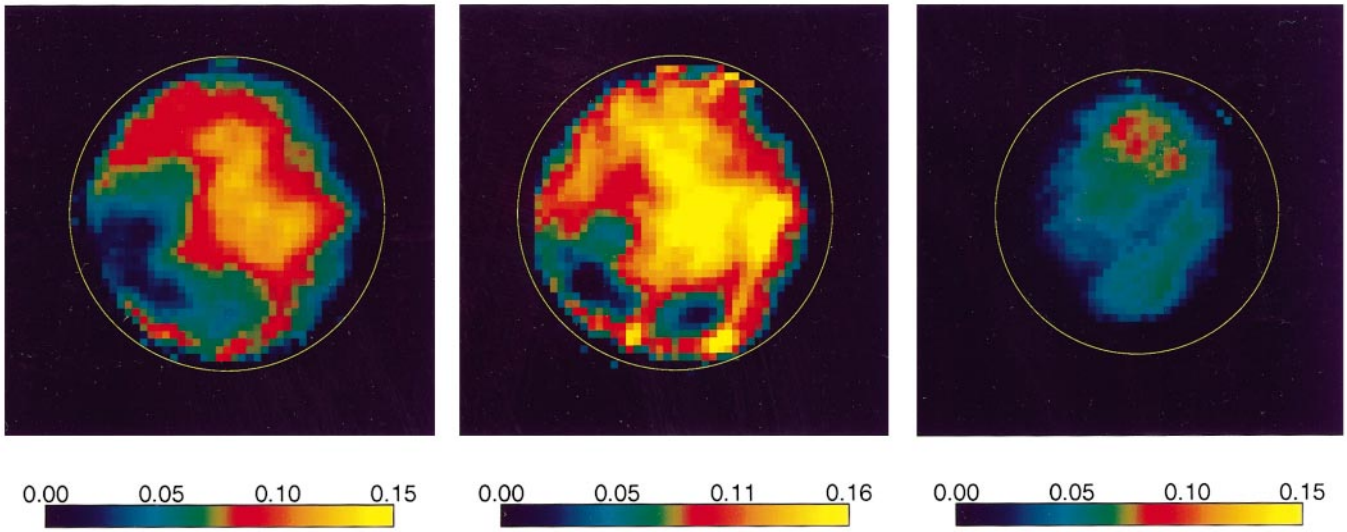

7

2.1 μm reflectance (20% less haze) 2.1 μm reflectance 2.1 μm reflectance (20% more haze)

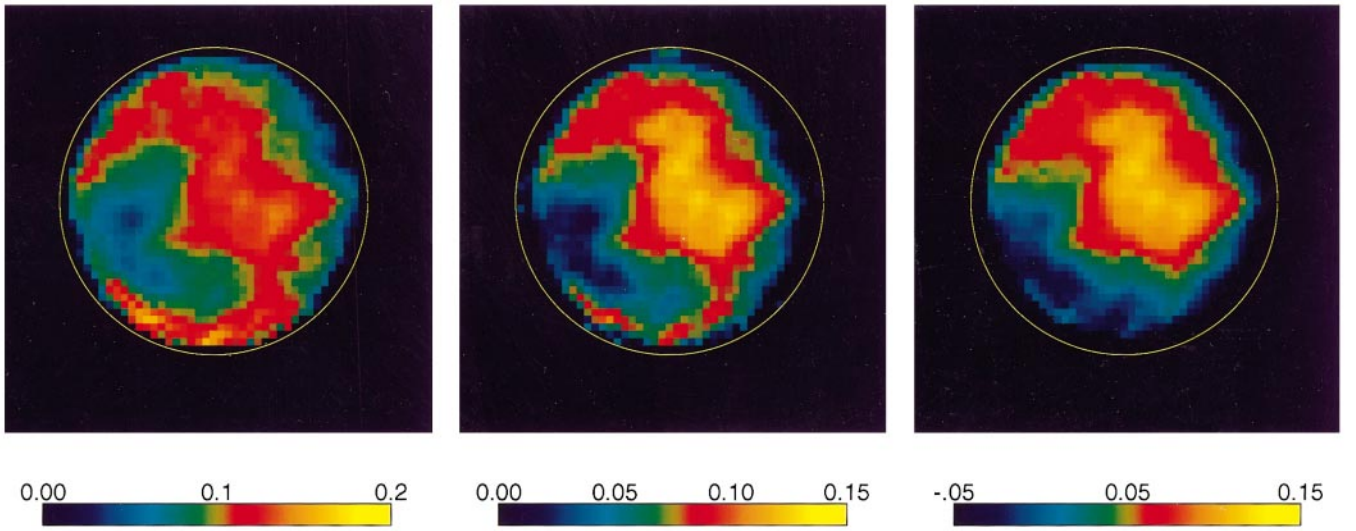

From what we know of Titan's atmosphere it seems likely that Titan's surface is continually impacted by material from above, whether in solid or liquid form. The fate of this material, whether washed to low-lying areas by methane rain, collected in underground reservoirs, or accumulating as liquid on the surface, remains uncertain.

7. CONCLUSIONS

Observations of Titan using speckle imaging at the W. M. Keck 10-m telescope have achieved a higher contrast and spatial resolution than previous images. They clearly show a variety of surface features on Titan and yield detailed information about the optical properties of Titan's atmosphere. Atmospheric modeling indicates haze optical depths at H and K′ that are smaller than predicted by spherical or fractal particle models. The north–south asymmetry in atmospheric brightness suggests a large difference in haze density in the two hemispheres which would be expected with seasonally dependent global circulation (Hourdin *et al.* 1995). Variations in surface reflectance, on scales that can only be resolved by high-resolution imaging, indicate a highly heterogenous surface, including bright areas consistent with ice or rock–ice, and dark areas with reflectance <0.05 which may be covered with organic solids or liquid hydrocarbons.

ACKNOWLEDGMENTS

We thank Ralph Lorenz, Athena Coustenis, and Mark Lemmon for the information they provided for this paper. Also, our thanks for the helpful comments of reviewers Caitlin Griffith and Chris Koresko. We also thank the staff of the Keck Observatory, particularly Wendy Harrison, for making these observations possible.

This research was performed under the auspices of the U.S. Department of Energy by Lawrence Livermore National Laboratory under Contract W-7405-ENG-48.

REFERENCES

Beletic, J. W., and R. M. Goody 1992. Recovery of planetary images by speckle imaging. *Appl. Opt.* **31**, 6909–6921.

Clark, R. N., and T. B. McCord 1980. The Galilean satellites: New near-infrared reflectance measurements (0.65–2.5 microns) and a 0.325–5 micron summary. *Icarus* **41**, 323–339.

Combes, M., A. Coustenis, L. Vapillon, E. Gendron, R. Wittemberg, and R. Sirdey 1996. Images of Titan's surface in the Near-IR with ADONIS. *Bull. Am. Astron. Soc.* DPS meeting no. 28, no. 20.04.

Combes, M., L. Vapillon, E. Gendron, A. Coustenis, O. Lai, R. Wittemberg, and R. Sirdey 1997. Spatially resolved images of Titan by means of adaptive optics. *Icarus* **129**, 482–497.

Degewij, J., D. P. Cruikshank, and W. K. Hartmann 1980. Near-infrared colorimetry of J6 Himalia and S9 Phoebe: A summary of 0.3–2.2 μm reflectances. *Icarus* **44**, 541–547.

de Pater, I., P. Palmer, D. L. Mitchell, S. J. Ostro, D. K. Yeomans, and L. E. Snyder 1994. Radar aperture synthesis observations of asteroids. *Icarus* **111**, 489–502.

Ghez, A. M., A. J. Weinberger, G. Neugebauer, K. Matthews, and D. W. McCarthy, Jr. 1995. Speckle imaging measurements of the relative tangential velocities of the components of T Tauri binary stars. *Astron. J.* **110**, 753–765.

Griffith, C. A., T. Owen, and R. Wagener 1991. Titan's surface and troposphere, investigated with ground-based near-infrared observations. *Icarus* **93**, 362–378.

Henry, T. J., and D. W. McCarthy 1993. The mass-luminosity relation for stars of mass 1.0 to 0.08 solar mass. *Astron. J.* **106**, 773–789.

Hourdin, F., O. Talagrand, R. Sadourny, R. Courtin, D. Gautier, and C. P. McKay 1995. Numerical simulation of the general circulation of the atmosphere of Titan. *Icarus* **117**, 358–374.

Hutzell, W. T., C. P. McKay, and O. B. Toon 1993. Effects of time-varying haze production on Titan's geometric albedo. *Icarus* **105**, 162–174.

Hutzell, W. T., C. P. McKay, O. B. Toon, and F. Hourdin 1996. Simulations of Titan's brightness by a two-dimensional haze model. *Icarus* **119**, 112–129.

Khare, B. N., C. Sagan, E. T. Arakawa, F. Suits, T. A. Callcott, and M. W. Williams 1984. Optical constants of organic tholins produced in a simulated titanian atmosphere: From soft X-ray to microwave frequencies. *Icarus* **60**, 127–137.

Khare, B. N., W. R. Thompson, C. Sagan, E. T. Arakawa, and J. J. Lawn 1990. Optical constants of solid ethane from 0.4 to 2.5 μm. *Bull. Am. Astron. Soc.* **22**, 1033.

Knox, K. T., and B. J. Thompson 1974. Recovery of images from atmospherically degraded short-exposure photographs. *Astrophys. J.* **193**, L45–48.

Koresko, C., S. Beckwith, A. Ghez, K. Matthews, and G. Neugebauer 1991. An infrared companion to *Z* Canis Majoris. *Astron. J.* **102**, 2073–2078.

Labeyrie, A. 1970. Attainment of diffraction limited resolution in large telescopes by Fourier analysing speckle patterns in star images. *Astron. Astophys.* **6**, 85–87.

Lara, L. M., R. D. Lorenz, and R. Rodrigo 1994. Liquids and solids on the surface of Titan: Results of a new photochemical model. *Planet. Space Sci.* **41**, 5–14.

Lawrence, T. W., D. M. Goodman, E. M. Johansson, and J. P. Fitch 1992. Speckle imaging of satellites at the Air Force Maui optical station. *Appl. Opt.* **31**, 6307–6321.

Lebofsky, L. A., M. A. Feierberg, and A. T. Tokunaga 1982. Infrared observations of the dark side of Iapetus. *Icarus* **49**, 382–386.

Leinert, C., H. Zinnercker, N. Weitzel, J. Christou, S. T. Ridgway, R. Jameson, M. Haas, and R. Lenzen 1993. A systematic approach for young binaries in Taurus. *Astron. Astrophys.* **278**, 129–149.

Lemmon, M. T., E. Karkoschka, and M. Tomasko 1995. Titan's rotation: Surface feature observed. *Icarus* **113**, 27–38.

Lockwood, G. W., B. L. Lutz, D. T. Thompson, and S. E. Bus 1986. The albedo of Titan. *Astrophys. J.* **303**, 511–520.

FIG. 6. Maps of Titan's surface reflectance. (a) is the leading hemisphere at K′; (b) shows the leading hemisphere at H; and (c) shows the trailing hemisphere at K′.

FIG. 7. Recovered surface reflectance for models with 20% less haze optical depth than the nominal value (a), 20% more haze optical depth (c), and the nominal value (b, nominal values are given in Table I). The model with 20% less haze shows clear undersubtraction of the southern limb, but the darkest reflectances are still <0.05. The model with 20% more haze produces surface reflectance in the dark regions that is <0, which is clearly unphysical.

Lohmann, A., G. Weigelt, and B. Wirnitzer 1983. Speckle masking in astronomy—Triple correlation theory and applications. *Appl. Opt.* **22**, 4028–4037.

Lorenz, R. D., and J. I. Lunine 1997. Titan's surface reviewed: The nature of the bright and dark terrain. *Planet. Space Sci.* **45**, 981–992.

Lorenz, R. D., C. P. McKay, and J. I. Lunine 1997. Photochemically driven collapse of Titan's atmosphere. *Science* **275**, 642–644.

Lunine, J. I., D. J. Stevenson, and Y. L. Yung 1983. Ethane ocean on Titan. *Science* **222**, 1229–1230.

Matthews, K., and B. T. Soifer 1994. The near-infrared camera on the W. M. Keck Telescope. In *Infrared Astronomy with Arrays: The Next Generation* (I. McLean, Ed.), pp. 239–246. Kluwer, Dordrecht.

Matthews, K., A. M. Ghez, A. J. Weinberger, and G. Neugebauer 1996. The first diffraction-limited images from the W. M. Keck Telescope. *Publ. Astron. Soc. Pacific* **108**, 615–619.

Max, C. E., D. Gavel, E. Johansson, B. Sherwood, M. Liu and B. Bradford 1996. Observations of Comet P/Shoemaker–Levy 9 impact on Jupiter from Lick Observatory using a high resolution speckle imaging camera. Presented at IAU Colloquium 156, Baltimore, MD May 9–12, 1995. [Also available as a technical report, Lawrence Livermore National Laboratory, Livermore, CA]

McAlister, H. A., W. I. Hartkopf, B. J. Gaston, E. M. Hendry, and F. C. Fekel 1984. Speckle interferometric measurements of binary stars. IX. *Astrophys. J. Suppl.* **54**, 251–257.

McCarthy, D. W., J. D. Freeman, and J. D. Drummond 1994. High resolution images of Vesta at 1.65 microns. *Icarus* **108**, 285–297.

McKay, C. P., J. B. Pollack, and R. Courtin 1989. The thermal structure of Titan's atmosphere. *Icarus* **80**, 23–53.

Muhleman, D. O., A. W. Grossman, and B. J. Butler 1995. Radar investigations of Mars, Mercury, and Titan. *Annu. Rev. Earth Planet. Sci.* **23**, 337–374.

Muhleman, D. O., A. W. Grossman, B. J. Butler, and M. A. Slade 1991. Radar reflectivity of Titan. *Science* **248**, 975–980.

Olivares, R. O. 1994. The application of infrared speckle interferometry to the imaging of remote galaxies and AGN. In *Astronomical Society of the Pacific, Airborne Astronomy Symposium on the Galactic Ecosystem: From Gas to Stars to Dust*, Vol. 73, pp. 197–198. Astronomical Society of the Pacific.

Rages, K., J. B. Pollack, and P. H. Smith 1983. Size estimates of Titan's aerosols based on Voyager high-phase-angle images. *J. Geophys. Res.* **88**, 8721–8728.

Rannou, P., M. Cabane, E. Chassefiere, R. Botet, C. P. McKay, and R. Courtin 1995. Titan's geometric albedo: Role of the fractal structure of the aerosols. *Icarus* **118**, 355–372.

Roddier, F. 1986. Triple correlation as a phase closure technique. *Opt. Commun.* **60**, 145–148.

Sagan, C., and S. F. Dermott 1982. The tides in the seas of Titan. *Nature* **300**, 731–733.

Sears, W. D. 1995. Tidal dissipation on Titan. *Icarus* **113**, 39–56.

Smith, P. H., M. T. Lemmon, R. D. Lorenz, L. A. Sormovksy, J. J. Caldwell, and M. D. Allison 1996. Titan's surface, revealed by HST imaging. *Icarus* **119**, 336–349.

Thatte, N., A. Quirrenbach, R. Genzel, R. Maiolino, and M. Tecza 1997. The Nuclear Stellar Core, the Hot Dust Source, and the Location of the Nucleus of NGC 1068. *Astron. J.* **490**, 238–246.

Tholen, D. J., and M. A. Barucci 1989. Asteroid taxonomy. In *Asteroids II* (R. P. Binzel, T. Gehrels, and M. S. Matthews, Eds.), pp. 298–315. University of Arizona Press, Tucson.

Toon, O. B., C. P. McKay, T. P. Ackerman, and K. Santhanam 1989. Rapid calculation of radiative heating rates and photodissociation rates in inhomogenous multiple scattering atmosphere. *J. Geophys. Res.* **94**, 16,287–16,301.

Toon, O. B., C. P. McKay, C. A. Griffith, and R. P. Turco 1992. A physical model of Titan's aerosols. *Icarus* **95**, 24–53.

Vilas, F., S. M. Larson, K. R. Stockstill, and M. J. Gaffey 1996. Unraveling the zebra: Clues to the Iapetus dark material composition. *Icarus* **124**, 262–267.

Von der Luehe, O. 1994. Speckle imaging of solar small scale structure. 2: Study of small scale structure in active regions. *Astron. Astrophys.* **281**, 889–910.

Weigelt, G. P. 1977. Modified astronomical speckle interferometry 'speckle masking.' *Opt. Commun.* **21**, 55–59.

Yung, Y. L., M. Allen, and J. P. Pinto 1984. Photochemistry of the atmosphere of Titan: Comparison between model and observations. *Astrophys. J.* (Suppl. Ser.) **55**, 465–506.